OCEAN MODELLING STUDIES IN SUPPORT OF ALTIMETRY

PAULA BERRY and JOHN MARSHALL

Space and Atmospheric Physics Group, Department of Physics, and Centre for Remote Sensing, Imperial College, London SW7 2BZ (Gt. Britain)

ABSTRACT

Berry, P. and Marshall, J., 1989. Ocean modelling studies in support of altimetry. Dyn.
  Atmos. Oceans, 13: 269–300

    Simulation studies are presented that consider the degree to which baroclinic ocean
circulation models are constrained by observations of the surface pressure field on space and
time-scales possible with future satellite-borne altimeters. Two- and three-layer eddy resolv-
ing quasi-geostrophic models are used to simulate and assimilate altimetric observations.
    For synoptic mapping of the oceanic eddy field on the scale of an ocean basin, a satellite
orbit repeat time of 14 days is found to be optimum. Our studies suggest that altimetric
observations will provide strong constraints on the surface flow of such models and, if used in
conjunction with them, may be used to infer the deep flows.

1. INTRODUCTION

    Satellite altimetry offers the prospect of global coverage of surface geo-
strophic currents on synoptic time-scales, and as such could play a central
role in future oceanographic observing campaigns. Perhaps the only way of
making sense of the information provided by altimeters and blending it in a
dynamically consistent way with other types of data, is by assimilation into
dynamical ocean models in much the same way as meteorologists form their
analyses.
    Assimilation of global data sets into global ocean models is not a realistic
possibility at present. For the immediate future we must proceed in stages
investigating regional problems with ocean models tailored to the prevailing
local dynamics. In the present contribution some aspects of synoptic map-
ping of geostrophic eddies from altimetry are considered by assimilation
into a multi-layer quasi-geostrophic ocean model.

A synoptic description of the oceanic geostrophic eddy field has as its aim a sequence of instantaneous maps at high spatial (10–100 km) and temporal (weeks–months) resolution. The altimeter has the potential to provide an appropriate data set for mapping the surface signature of the oceanic eddy field. This particular application of altimetry is considered here because we believe it to be a feasible one, rather than because it should necessarily be regarded as having a high scientific priority. The geostrophic eddy field has a strong surface-height signal and is of small horizontal scale and so is associated with pronounced sea-surface tilts. Systematic long wavelength uncertainties in tides and satellite orbits, which may compromise our ability to monitor the gyre-scale circulation, may not be limiting on the synoptic-scale. Further, detailed gravimetric geoids exist for the western North Atlantic whose errors do not appear to swamp the oceanographic signal, suggesting that absolute velocity determination may be a possibility (see Cheney and Marsh, 1981). Finally, since the geostrophic eddy field is a dynamical instability of the larger scale flow, and is rather well described by the conservation of potential vorticity on synoptic time-scales, our dynamical understanding is arguably sufficient to contemplate the use of numerical models to assimilate the height-field data.

A less ambitious, but nevertheless valuable application of models lies in observing system simulation studies where they can be used to optimize the deployment of observing platforms. For example, in altimetry there needs to be a compromise between spatial and temporal coverage. Models can help us arrive at optimum specifications for, say, synoptic mapping of Gulf Stream variability.

Our investigation assesses the degree to which observations of the surface pressure field on the space and time-scales possible with a satellite-borne radar altimeter are useful in constraining eddy resolving, basin-scale ocean circulation models. Our study is the first, we believe, to contemplate assimilation into basin-scale models that simultaneously resolve the synoptic eddy field. Observing system simulation studies are presented which suggest that such data will provide strong constraints on the surface flow in a baroclinic model, and allow us to infer the deep flow.

In section 2 the rationale for using dynamical models as a vehicle for blending diverse data types is set out, stressing the importance of the model as a source of a priori information. The objective analysis technique employed to blend model and data is introduced. In section 3 an ocean model is briefly described and in section 4 observing system simulation studies with two and three-layer versions of the model are presented. A mechanism by which information at the surface is projected vertically is proposed and provides the dynamical background used to interpret the data assimilation experiments.

2. THE USE OF MODELS IN THE ANALYSIS OF DATA

Oceanographic data are of many types, of varying quality and is irregularly distributed in space and time. The observing system is improving but it will always be incomplete and subject to errors, much more so than the meteorological network, for in the ocean there are almost insurmountable sampling problems. From these observations a best estimate of the true state of the ocean is to be constructed. Because of the sparcity of the data and their inaccuracy there are an infinite number of ocean states consistent with the observations and so there is no alternative but to rely heavily on a priori information in deciding which ocean state is most likely. Minimum variance estimation, a tried and tested method of optimally combining observations with a priori information, is now outlined in a context that is familiar to oceanographers and in a manner which makes transparent the use of prior knowledge (for a very useful introduction to the theory see Ghil et. al. (1981)). The technique will be employed to blend model and data in our simulation studies of sections 3 and 4.

2.1. Minimum variance estimation

Suppose $\mathbf{u}$ are variables representing the state of the ocean on a regular grid (dimension n) and there are incomplete and regularly spaced observations of $\mathbf{u}$, $\mathbf{z}$ (dimension $= p$, $p < n$), contaminated by errors

$$z = \mathbf{A}u + \epsilon \tag{1}$$

where $\mathbf{A}$ is a matrix representing the process of taking an observation and ϵ is the error in that observation. The z could be expendable bathythermograph measurements of temperature and salinity, velocities measured by current meters, satellite observations of the ocean topography and wind-stress curl, etc.

For example, in Fig. 1 (showing the upper layer stream function from an eddy-resolving model), the $\mathbf{u}$ would correspond to the values of the streamfunction at the grid points in each layer of the numerical model and z would correspond to the (simulated) satellite observations of the upper layer along the selected tracks indicated by the criss-crossing black lines. Since some function of the variable may be observed rather than the analysis variable itself, the entries of $\mathbf{A}$ need not be 0 or 1. However, in our simple case $\mathbf{A}$ is made up of only 0s and 1s and has a particularly simple form reflecting the regular spatial pattern of the (repeated) satellite tracks. From these observations, $\mathbf{z}$, our object is to make the best estimate of $\mathbf{u}$, $\hat{\mathbf{u}}$.

Accordingly we look for an estimator $\mathbf{H}$ which operates on the data

$$\hat{u} = \mathbf{H}z \tag{2}$$

(a)

(b)
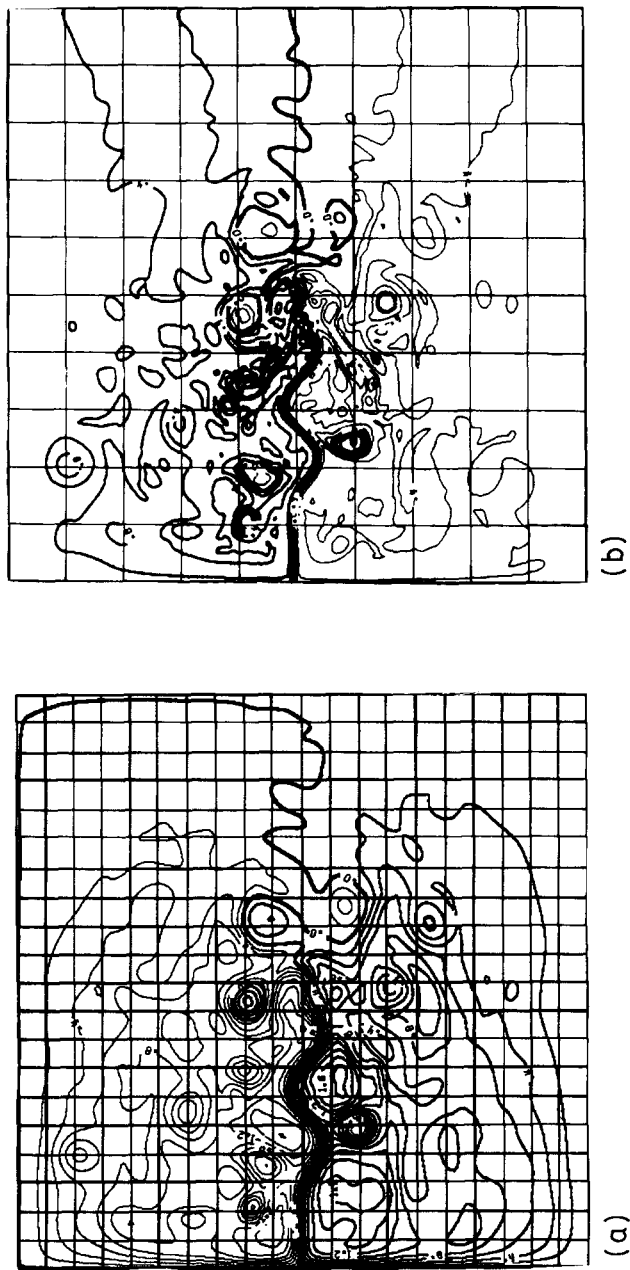
Fig. 1. (a) Upper layer streamfunction from the two-layer model 'truth' circulation on day 108; the contour interval (CI) is 5 cm of ocean topography. The tracks from a simulated 14-day repeat orbit are superimposed. (b) Corresponding upper layer quasi-geostrophic potential vorticity (non-dimensional units).

to give an estimate of **u**, **û**. To derive an optimum **H** (in the sense of least squares) we form the covariance of the estimated error (from eqns. (1) and (2)) and choose the one that minimizes its trace. This optimum **H** is (see, for example, Rodgers (1976) or Ghil et al. (1981) and references therein)

$$\mathbf{H} = \left(\mathbf{A}^T\mathbf{C}_\epsilon^{-1}\mathbf{A} + \mathbf{C}_u^{-1}\right)^{-1}\mathbf{A}^T\mathbf{C}_\epsilon^{-1} \tag{3}$$

the well known minimum variance estimator, where $\mathbf{C}_u$ is the covariance of u, and $\mathbf{C}_\epsilon$ is the covariance of the observing errors.

Of all the linear estimators, eqn. (3) is the best in the sense of least squares. Substituting eqn. (3) into eqn. (2), gives an estimate

$$\hat{\mathbf{u}} = \mathbf{C}_u\mathbf{A}^T\left(\mathbf{A}\mathbf{C}_u\mathbf{A}^T + \mathbf{C}_\epsilon\right)^{-1}\mathbf{z}$$

$$= \left(\mathbf{A}^T\mathbf{C}_\epsilon^{-1}\mathbf{A} + \mathbf{C}_u^{-1}\right)^{-1}\mathbf{A}^T\mathbf{C}_\epsilon^{-1}\mathbf{z} \tag{4}$$

with an expected error

$$\mathbf{C}_{\hat{u}-u} = \left(\mathbf{A}^T\mathbf{C}_\epsilon^{-1}\mathbf{A} + \mathbf{C}_u^{-1}\right)^{-1} \tag{5}$$

Equation (4) is useful if we are willing to make a priori assertions concerning the spatial correlations and amplitude of the field **u** (i.e., if there is a priori knowledge of $\mathbf{C}_u$), for it describes how to weight the observations in an optimum way. How good the best estimate is depends on our ability to make useful statements about the statistics of **u** and the observational errors (within the limitations of the data).

If, however, we are not prepared to make any statements about the solution covariance at all, but have information only about the statistics of the observational errors ($\mathbf{C}_\epsilon$ is assumed known) then eqn. (4) reduces to (as $\mathbf{C}_u \rightarrow \infty$)

$$\hat{\mathbf{u}} = \left(\mathbf{A}^T\mathbf{C}_\epsilon^{-1}\mathbf{A}\right)^{-1}\mathbf{A}^T\mathbf{C}_\epsilon^{-1}\mathbf{z} \tag{6}$$

Equation (6) will be useful in section 2.2, when a priori information, for example as provided by an ocean model, is treated as data.

In most situations, though, the minimum of information solution (eqn. (6)) can be improved because there is a priori information about the variance and spatial correlation of **z**. This comes from past observations and dynamical understanding and can be used to make useful statements about $\mathbf{C}_u$ enabling our estimate to proceed via eqn. (4).

In the present context our object is to synoptically map the geostrophic eddy field exploiting altimetry and an ocean model. On synoptic time-scales the dynamics is governed by the close conservation of potential vorticity (see section 3). The preferred scale of ocean eddies is on the Rossby radius of deformation, $L = NH_e/f$, where H_e is the equivalent depth of a vertical

mode (first baroclinic, say), N is a measure of the stratification and f is the Coriolis parameter. Even though our knowledge of geostrophic eddy dynamics may be incomplete and our statements therefore not very precise, it is nevertheless useful information with which to guide our choice of C_u. In this way, prior knowledge of ocean dynamics is brought to bear in the analysis of the observations, constraining the number of possible solutions.

For instance, a particularly simple, yet useful, form of the correlation is the Gaussian covariance structure function

$$F(\xi) = e^{-\frac{1}{2}(\xi/b)^2}$$

where $F(\xi) = \langle [u(r) - \bar{u}][u(r + \xi) - \bar{u}] \rangle$ and $\bar{u}$ is the mean. $F(\xi)$ is the average over all r of two values of $\mathbf{u}$ separated by a distance ξ. The correlation scale, b, is set by the spatial scale of the field $\mathbf{u}$, of the order of the Rossby radius for the oceanic synoptic scale.

It is important that the covariance structure function be chosen carefully, since it determines the scales in the data that are enhanced in the estimate, and also how the information is interpolated between data points. The way in which the estimator $\mathbf{H}$ weights the various scales in the data can be made transparent by looking at the eigenvectors and eigenvalues of C_u; this is discussed further in, for example, Rodgers (1976), Hollingsworth (1984) and, in the present context, by Marshall (1985a). Using such techniques, it can be shown that if a Gaussian covariance is chosen for C_u, and this is combined with a diagonal covariance $C_\epsilon = \sigma_0^2 I$ for random, uncorrelated error, $\mathbf{H}$ will always smooth the data, the extent to which it does so being dependent on b.

2.2. Models as a source of a priori information

The minimum variance estimator (eqn. (4)) is very useful if our a priori information is only of a statistical nature, but a potentially more powerful and direct use of our dynamical understanding would be to use a dynamical model to provide a priori information about the field, u, in addition to its statistics, i.e., to use it as a 'first guess'. This will be of particular value in the oceanographic context because the interpolation problems are so acute that all our prior knowledge of ocean dynamics must be brought to bear in the interpolation procedure to make the best use of the data available. Since the ocean model is the most concise statement of this knowledge, it seems natural to use it as an analysis tool. In such an approach the ocean model provides a first guess of $\mathbf{u}$, which we will call $\hat{u}(-)$, adopting the notation of Ghil et al. (1981). It is enlightening to regard the first guess as a 'virtual observation' that is of the same nature as the field observations, but which differs only in its error characteristics; for a more detailed discussion from

this perspective see Marshall (1985a). Virtual observations can be treated explicitly as data by augmenting the data eqn. (1) thus

$$\hat{u}(-) = Iu + \epsilon_{\hat{u}} \tag{7}$$

Here the ocean model is being used as a measuring instrument providing a first guess of u, with an error $\epsilon_{\hat{u}}$ that is assumed independent of the observations. When observations z of u become available they are combined with a first guess to form a better estimate of u, $\hat{u}(+)$. So eqns. (1) and (7) are combined to give (following Jackson, 1979)

$$z_* = A_* u + \epsilon_* \tag{8}$$

where

$$z_* = \begin{pmatrix} z \\ \hat{u}(-) \end{pmatrix}; \qquad A_* = \begin{pmatrix} A \\ I \end{pmatrix}$$

and

$$\epsilon_* = \begin{pmatrix} \epsilon \\ \epsilon_{\hat{u}} \end{pmatrix}$$

The covariance of data errors $C_{e*} = E(\epsilon\epsilon^T_*)$ is

$$C_{\epsilon*} = \begin{pmatrix} C_\epsilon & 0 \\ 0 & U \end{pmatrix}$$

where $U = E(\epsilon_{\hat{u}}\epsilon^T_{\hat{u}})$ is the covariance of the ocean model errors and $C_\epsilon = E(\epsilon\epsilon^T)$ is the covariance of errors in the observations.

Equation (8) demonstrates clearly how the use of a priori information has changed the original underdetermined problem, eqn. (1), into an overdetermined problem ($n + p > n$) with a unique solution. Because our a priori information has been treated as data, eqn. (8) can be solved using eqn. (6) to give a new, improved estimate

$$\hat{u}(+) = \left(A^T C_\epsilon^{-1} A + U^{-1}\right)^{-1}\left[A^T C_\epsilon^{-1} z + U^{-1}\hat{u}(-)\right] \tag{9a}$$

with expected error

$$U_+ = \left(A^T C_\epsilon^{-1} A + U^{-1}\right)^{-1} \tag{9b}$$

This is the most general form of minimum variance estimator. Equation (5) is a special case of eqn. (9) with $\hat{u}(-) = 0$.

Before proceeding further it should be emphasized that all a priori information can be treated as virtual observations (dynamical constraints, smoothness criteria, climatology, etc.) by writing it in the form (8). This is an enlightening perspective from which to view a priori information. In eqn. (5) the 'virtual observation' was $\hat{u}(-) = 0$ and the expected error in this observation was U.

Although at first sight eqn. (9) looks rather complicated, it is nothing more than a straightforward generalization of the well-known scalar formula

$$\text{estimate} = \frac{\sum(\text{observation}/\text{error in observation})}{\sum(1/\text{error})}$$

Not surprisingly the best estimate weights the observations (real and virtual) with respect to their error covariances.

2.3. Optimum interpolation

Equation (9) involves the inversion of large ($n \times n$) matrices and so is of limited practical use. However it can be written in a less computationally taxing form thus (see, for example, Rodgers (1976))

$$\hat{u}(+) = \hat{u}(-) + K[z - A\hat{u}(-)] \tag{10a}$$

where

$$K = UA^T(AUA^T + C_\epsilon)^{-1} \tag{10b}$$

is a matrix of weighting coefficients. Unlike eqn. (9), eqn. (10) only involves the inversion of ($p \times p$) matrices, where p is the number of observations. It relates the correction to the first guess to observed deviations from it, through the matrix K. Information about the geometrical configuration of the observation and estimation points is contained in the covariances, and our choice of U determines how the data are interpolated spatially. Equation (10) has been derived on numerous occasions and applied in many diverse fields. It is the inverse method used by Wunsch (1978) to determine the ocean circulation from hydrographic sections. Equation (10) is the general form in which linear estimation is applied in meteorological interpolation, where it is known as objective analysis. It was first introduced into the meteorological literature by Eliassen (1954) and later developed by Gandin (1965). The most systematic and concerted effort to apply objective techniques combining dynamical models and data in an oceanic context is that due to Robinson and collaborators (see Robinson (1986) for a review).

Equation (10) sets out a general procedure to combine observations and a priori constraints optimally. We now describe in more detail how the formalism could be used to blend observations of ocean topography from altimetry with virtual observations provided by an eddy resolving model to synoptically map the geostrophic eddy field. As in the meteorological application of eqn. (10), instead of adopting climatology as a first guess, a model is used to provide a short-range forecast interpolating information in space and time. In this way the forecast provides information about the

field, and so can be regarded as a measuring instrument just like the altimeter. The philosophy behind the use of a dynamical model in this way is based on the assumption that the information provided by it is close in some sense to the truth (i.e., the model has some skill). It is then reasonable to linearize the inversion about the first guess as assumed in eqn. (10a).

3. OBSERVING SYSTEM SIMULATION STUDIES

3.1. The ocean model

We briefly describe an eddy-resolving circulation model of the Gulf Stream and its recirculation, which is used to establish a 'truth' or 'reference' circulation. This is sampled to simulate an altimetric data set and a degraded version of the model is subsequently employed to assimilate the data.

The ocean is an N layer quasi-geostrophic model confined to a rectangular basin on a β-plane, and governed by the quasi-geostrophic potential vorticity equation. Data assimilation experiments have been carried out with two- and three-layer versions of the model. The circulation is driven by an imposed wind-stress curl and frictionally retarded

$$\frac{\partial q}{\partial t} + J(\psi, q) = G \tag{11}$$

where q is the quasi-geostrophic potential vorticity, ψ is the streamfunction, and G are potential vorticity sources and sinks.

A finite-difference version of eqn. (11) is stepped forward from a known initial state in a double gyre configuration

$$0 \leq x \leq L$$
$$-0.5L \leq y \leq 0.5L$$

with

$$\nabla \wedge (\text{wind stress}) = \tau_0 \sin(2\pi y / L)$$

to generate a reference 6-month sequence of 'synoptic' maps of the Gulf Stream and its recirculation. Details of the numerical implementation can be found in Brugge et al. (1987). Model parameters are given in the Appendix.

Figure 1 shows the streamfunction (a) and potential vorticity (b) in the uppermost layer of a two-layer integration in a 3000 × 3000 km basin. An unstable internal jet flows eastward parallel to the front in the potential vorticity field, separating subpolar and subtropical gyres. The scale of the eddying motion is set by the Rossby radius of deformation ($\sim$ 48 km); the eddies have a strong pressure signal and so are associated with pronounced

sea-surface slopes. In Fig. 1 the sea-surface drops by about 1 m, moving northwards across the eastward flowing Gulf Stream. The time-scale of the eddying motion is of the order of weeks and months; cut-off warm and cold rings with closed potential vorticity contours (indicating material transfer of fluid across the front) are particularly long lived. Inspection of grey-scale movie sequences of the potential vorticity field reveals a wealth of dynamical activity: there is evidence of Rossby wave radiation from the meandering Gulf Stream, Rossby wave breaking, ring formation, spontaneous generation of vortex pairs, etc. In common with all quasi-geostrophic models there is perhaps less of a proclivity for loops to pinch-off from the Stream: as can be seen in Fig. 1b the internal jet remains rather contiguous. Furthermore, in this two-layer integration the eddy activity tends to be concentrated in the region of the internal jet and is not prevalent in the interior of the gyre. However, in the experiments presented in section 4.5, with a three-layer model, the interior of the gyre is also explicitly unstable and the eddy activity more uniformly distributed over the basin.

Despite the limitations of the quasi-geostrophic formulation, it has several advantages over other perhaps more realistic models with more degrees of freedom. If it is assumed (consistently with the layered formulation) that the horizontal velocity does not vary with depth within the layer, then the upper layer streamfunction can be interpreted in terms of the ocean topography, the deviation of the sea surface from the gravimetric geoid $h = (f/g)\psi$, where f is the Coriolis parameter and g is the acceleration due to gravity. Thus the model can assimilate height field data in an obvious way. Furthermore, because it is a filtered model, it does not suffer from initialization problems associated with spurious gravity wave activity generated by noisy data. Finally, the model has space and time-scales in common with the oceanic synoptic scale; the flow depicted in Fig. 1 has many realistic features both in the mean and eddy characteristics.

3.2. Sampling strategy

On reaching a statistically steady state, the model is integrated forward to generate a reference 6-month sequence of 'synoptic' maps of the eddying Gulf Stream and its recirculation. This is our 'truth' circulation, which is then sampled to simulate the altimetric data set.

The 'truth' circulation is sampled, simulating the spatial density and temporal frequency of the tracks laid down by a satellite in an exactly repeating orbit. For such an orbit, with period τ_{rev} and repeat time T, there are T/τ_{rev} revolutions per repeat cycle, giving a track spacing at the Equator of

$$d = \frac{360}{T/\tau_{rev}} \quad \text{(degrees)}$$

TABLE I

Repeat times and track spacings for a satellite in an 800-km-altitude orbit

Repeat time (days)	Track separation at 45° North (d (km))	d/2b [a]
10	200	1.3
14	140	0.9
30	63	0.4

[a] b is the correlation scale (78 km) used in the simulation experiments.

Thus the temporal and spatial resolutions are limited by

$$d \times T = 360 \tau_{rev}$$

For SEASAT, which flew at an altitude of 800 km, $\tau_{rev} = 0.0698$ days, yielding the following approximate relationship between repeat-time and track spacing

$$\text{repeat time} \times \text{spacing between tracks at equator} \sim 24 \qquad (12)$$
$$\text{(days)} \qquad\qquad\qquad \text{(degrees)}$$

The spacing between the tracks decreases with the cosine of the latitude.

In our simulation studies the satellite is constrained to pass over columns and rows of the finite-difference grid, giving an independent measurement at each grid point along the track. To give an impression of the spatial resolution possible, simulated tracks on a 14-day repeat over the 3000 × 3000 km basin are shown in Fig. 1. Table I gives chosen track separations, d, as a function of repeat time. The satellite is flown over this grid, laying down its tracks in a pre-determined order; subsequent experiments were found to be insensitive to the details of this ordering.

It is assumed that after the required corrections (due to sea-state bias, atmospheric water vapour, atmospheric loading, ionospheric effects, etc.) have been made, there remains an irreducible random error, ϵ, in the sea-surface height measurement. It is supposed that errors due to orbital uncertainties and tides have sufficiently long wavelengths relative to the synoptic scale that they result in a systematic error along the track that can be eliminated. It should be emphasized that this is perhaps a rather optimistic assumption on the scale of the gyre since long-wavelength tracking errors may be difficult to separate from the mean circulation on scales of 3000–4000 km. Furthermore, no attempt is made to simulate the error in the gravimetric geoid, but we acknowledge that it is this spatially correlated error (of uncertain amplitude and scale), rather than the random errors, which will ultimately limit the potential of altimetry in ocean circulation studies. The combined problem of determining the ocean circulation whilst improving

the geoid, using ocean models in conjunction with altimetry, is discussed by Marshall (1985a).

Thus, our simulated observations of the deviation of the sea surface from the gravimetric geoid along a track are

$$\mathbf{z} = \mathbf{z}^{\mathrm{track}} + \boldsymbol{\epsilon} \tag{13}$$

where $\mathbf{h}^{\mathrm{track}}$ is taken from the 'truth' circulation and $\boldsymbol{\epsilon}$ is the random error component taken from a normal distribution with zero mean and standard deviation σ_0

$$\begin{aligned}\text{Expectation} \quad \mathbf{E}(\boldsymbol{\epsilon}\boldsymbol{\epsilon}^{\mathrm{T}}) &= \sigma_0^2 \mathbf{I} \\ \text{and} \quad \mathbf{E}(\boldsymbol{\epsilon}) &= \mathbf{0}\end{aligned} \tag{14}$$

Although eqn. (14) is a gross oversimplification of the expected errors (principally geoid and tracking) of the altimetric system, and will lead to over-optimistic results, it seems sensible here to adopt the simplest possible error structure to provide a base-line for future reference. For example it is by no means clear, a priori, that perfect observations of the surface pressure field on the space and time scales possible with a satellite-borne altimeter can constrain a highly non-linear eddy-resolving ocean circulation model such as the one employed here.

3.3. Analysis procedure

We now consider the problem of forming an estimate $\hat{\mathbf{h}}$ over the entire $I \times J$ grid from simulated observations repeated along selected tracks. As stressed in section 2 this is an underdetermined problem and so heavy reliance must be placed on a priori information.

A climatological field at the resolution of the grid could be chosen as a first guess together with an estimate of its error. But this is an understatement of our a priori knowledge because there is dynamical information that can be brought to bear in forming the best estimate. Having simulated the data by sampling an evolving flow governed by eqn. (11), it would be sensible to assimilate the observations into the same model. The model can then be employed to advect information between the repeated satellite tracks, thus projecting past information into the future. One should be wary, though, of only assimilating data into a perfect model. In reality there are many dynamical and physical processes that are not adequately described by an ocean model, and so there is a danger of over-optimistic results if the model that simulated the data is also used to assimilate it. To represent this model imperfection crudely, in section 4.4 degraded versions of eqn. (11) are also used to assimilate the data.

Thus the observations are augmented with an a priori estimate of **h** that would have been made in the absence of altimetry

$$\mathbf{z}_* = \begin{pmatrix} \mathbf{z} \\ \mathbf{h}(-) \end{pmatrix}$$

As discussed in section 2, the 'first guess' and the observations are optimally combined applying the least-squares procedures eqn. (10) (weighting with respect to error covariances of **z** and **h**(−)).

The following continuous updating strategy is employed:

(1) starting from a prescribed climatological initial state;

(2) the model is integrated forward in time providing an estimate of the ocean topography **h**(−), which is in error because of inadequacies in the model physics and the imperfectly known initial state;

(3) when the satellite flies overhead the observations **z** along a particular track are optimally combined with the estimate of the ocean topography currently carried by the model, **h**(−), to provide a (hopefully) better estimate of the true state of the ocean, **h**(+);

(4) the model is then integrated forward until the next observation time, when it again provides the first guess in step 3.

In this way, the model is used to extrapolate the information provided by the altimeter forward in time, whilst our objective mapping techniques interpolate between the tracks. The relative merits of various updating and observing strategies can be measured with reference to the truth circulation by, for example as chosen here, computing the root-mean-square-error (r.m.s.e.) between **h** and **ĥ**. Other objective measures can be chosen (see, for example, Rienecker et al. (1987)) but would not lead to qualitatively different conclusions.

Because the model is continuously updated and the satellite tracks are straight, the analysis problem eqn. (10) reduces to a series of one-dimensional ones. Each time the satellite passes overhead, estimates along and either side of the track are made. Fifteen data points equally spaced every 15 km along the track (at the resolution of the numerical model) are used to analyse for the ocean topography. The radius of influence of the data is determined by the correlation scale of the covariance matrix of the model first guess errors, chosen to be a Gaussian covariance structure function (see section 2). At distances from the track much greater than the correlation scale b, the analysis tends to the first guess, **h**(+) → **h**(−). We choose to update the model fields on either side of the track out to a distance of $2b$.

The performance of the analysis is rather sensitive to the choice of correlation scale. If b is too large, the analysed fields are too smooth and fail to capture the details of rings and eddies and frontal structures. Alternatively, if the correlation scale is too small, the impact of data insertion can

be detrimental since spurious, small-scale features are introduced into the analysis, which very rapidly approaches the first guess on either side of the satellite track. In our studies the optimum b was found empirically to be 78 km, somewhat less than twice the Rossby radius. This correlation scale was kept fixed and applied over the whole basin and at all times. It is doubtful that this assumption of stationary error covariance structure function is strictly valid in such a non-linear, non-stationary eddy field. More complicated (and realistic) error models could have been constructed, but the added computational effort involved in the implementation of such a scheme would not, in our opinion, have led to substantially improved results.

4. ALTIMETRIC DATA AS A CONSTRAINT ON BAROCLINIC CIRCULATION MODELS

4.1. Repeat-time strategies

Figure 2 shows the r.m.s.e. between $\mathbf{h}$ and $\hat{\mathbf{h}}$ as a function of time for various repeat-time strategies in the two-layer integration from which Fig. 1 is taken. For clarity only the upper layer curves are displayed. The impact of data on lower layers is considered in section 4.3. Such r.m.s.e. curves are often normalized with respect to the climatological variability. Here, however, it was thought that more information was conveyed by presenting the errors in absolute units: to normalize they should be compared with the no-data integration (curve A) which gives a measure of the natural variability. For each repeat-time the same amount of data (in toto) are supplied, only its spatial and temporal frequency differs (see eqn. (12)). Data were assimilated into the model (an identical twin, or perfect model) starting from a 'climatological' initial state, taken to be a linear Stommel (1948) solution in the upper layer of the model, with no flow beneath. Our results are not sensitive to our choice of initial conditions.

When no data are inserted , curve A, the r.m.s.e. between $\mathbf{h}$ and $\hat{\mathbf{h}}$ remains fairly steady at 8 cm. This is a useful reference since it is a measure of the variability of the model about climatology. It should be remembered that this is a basin-scale measure: the variance is concentrated in the region of the separated jet where it rises to as high as 30 cm r.m.s..

Assimilation of perfect data into the model on 10-, 14- and 30-day repeat cycles reduces the r.m.s.e. to about one-third of the natural variability about climatology. This in itself is a significant result since it demonstrates that observations from a single (albeit perfect) altimetric system are capable of constraining a two-layer eddy resolving basin-scale ocean circulation model. Although data are assimilated by the model continuously, the repeat fre-
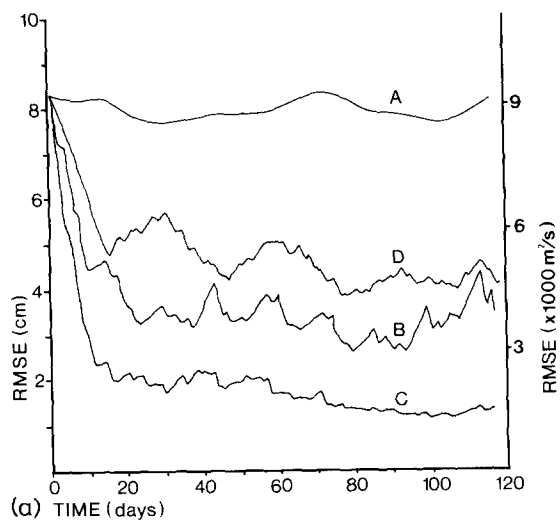
Fig. 2. (a) Root-mean-square error (r.m.s.e) between the truth and assimilation model ocean topographies from a two-layer model initialized with a Stommel solution in the upper layer and no motion beneath: Curve A, no data assimilated; curve B, data assimilated from a 10-day repeat orbit; curve C, data assimilated from a 14-day repeat orbit; curve D, data assimilated from a 30-day repeat orbit. Curve A is a measure of the variability of the model about the linear solution. (b) Analysis of upper layer streamfunction (14-day repeat) on day 108; CI = 5 cm of ocean topography.

quencies can be seen in the r.m.s.e. curves. This is because the error falls dramatically as the satellite flies over the model Gulf Stream where most of the variance is concentrated. Data in the quiescent interior region reduce the r.m.s.e. locally, but have only a small impact on the error in toto. Such considerations explain why, with a 30-day repeat (curve D), the error undergoes large fluctuations during its cycle. The satellite spends too much of its time in regions where the variance is small, allowing the model to deviate further from the truth.

A useful way of rationalizing the trade-off between space and time resolution is to consider the ratio $d/2b$, where d is the track separation, and b is the correlation scale of the signal (see Table I). Our experiments suggest that an optimum sampling strategy would make this ratio $d/2b \sim 1$. Indeed the r.m.s.e. is reduced to a minimum for a repeat-time of 14 days (curve C in Fig. 2) implying a track separation of 140 km, almost exactly twice the correlation scale b. This result was obtained earlier by Marshall (1985b), but by using a barotropically unstable one-layer ocean circulation model in a miniature ocean basin.

To give a visual impression of the success of the assimilation procedure the analysis of the upper layer streamfunction on day 108 of the assimilation using data from a 14-day repeat orbit is shown in Fig. 2b. A comparison with the truth for the same time (Fig. 1a) shows that the major features of the circulation are reproduced rather effectively in the analysis, and the upper layer flow is well constrained by data from one altimeter. Evidently,
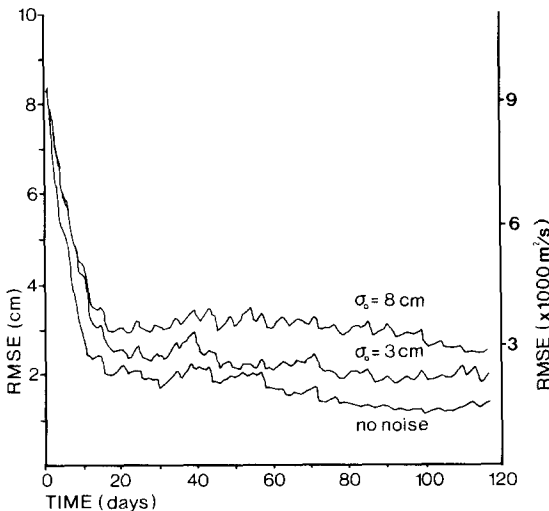
Fig. 3. Error curves for the ocean topography obtained by assimilating data with varying noise levels on a 14-day repeat into a two-layer model initialized as described in Fig. 2.

in a 30-day repeat-cycle, the satellite over-samples in space ($d/2b = 0.4$) at the expense of temporal resolution; the converse is true in a 10-day repeat orbit ($d/2b = 1.6$).

4.2. Impact of random data errors

Figure 3 demonstrates the insensitivity of the analysis error to (reasonable) random errors in the observations. In each case the repeat time is 14 days. A random error of 8 cm (r.m.s.) (a signal to noise ratio of unity) does not cause a significant deterioration in the analysis, since a Gaussian covariance results in a very effective smoothing weights matrix **K**. It should be no surprise that the analysis error can be less than the random error in each independent measurement because the interpolation procedure tends to average the observations over a correlation scale. Further, a wealth of a priori information is being brought to bear on the analysis through the use of eqn. (11), which encapsulates our dynamical understanding of the field.

4.3. Extrapolation of single-level data in the vertical

Given that remotely sensed data can only give direct information about properties of the ocean surface, one of the most important objectives of our study is to ascertain to what extent a dynamical model can be used in conjunction with altimetry to infer the subsurface flow. Aspects of this problem have been considered by Hurlbert (1985) in a limited-area model of the Gulf of Mexico.

Figure 4 presents the r.m.s.e. between the truth and analysis ψ_2 fields obtained by assimilating perfect data on a 14-day repeat into a two-layer perfect model initialized as described in section 4.1. Note that now, for this
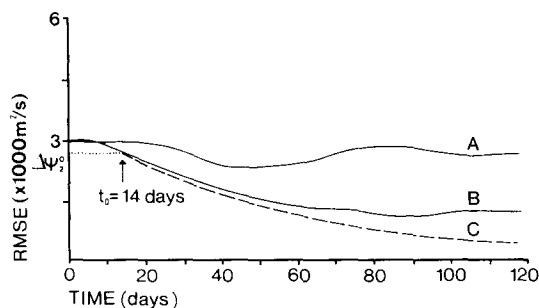
Fig. 4. Lower layer r.m.s.e. curves for the two-layer integration in Fig. 2. Curve A, r.m.s.e. in ψ_2 when no data are assimilated; curve B, r.m.s.e. in ψ_2 when perfect data are assimilated on a 14-day repeat; curve C, $\Delta\psi_2\exp[-\epsilon(t - t_0)]$: $t_0 = 14$ days, and $\Delta\psi_2(t_0)$ is the r.m.s.e. in ψ_2 at t_0.

Fig. 5. Lower layer streamfunctions from (a) truth and (b) assimilation (14-day repeat, perfect data, as in Fig. 2) two layer integrations on day 108; CI = 1500 m^2 s^{-1}. The thick black line is the zero contour.

subsurface layer, the vertical scale is expressed in dimensional streamfunction units of m^2 s^{-1}. No vertical extrapolation procedures are employed: rather the lower layer flow is allowed to evolve freely, adjusting to the continually updated surface flow. The lower layer r.m.s.e. is markedly reduced over a period of 100 days or so; inspection of the instantaneous flow patterns reveals that the position and scale of the eddy field is reproduced with some skill (see Fig. 5, which presents the lower layer truth and analysed fields after 60 days).

A plausible dynamical mechanism that accounts for the success represented by the curve in Fig. 4 is now emerging.

Energetic eddies in the upper layer (in and above the main thermocline) drive the deep flow through vertical motions, which act like 'plungers' rippling the interface on the scale of 100–200 km, generating Rossby waves in the lower layer (see, for example, Rhines and Holland (1979) or Haidvogel and Rhines (1983)). The lower layer of the two-layer model is deep and the currents weak and so non-linear processes do not dominate.

Accordingly, suppose that the lower layer vorticity equation can be linearized thus

$$\frac{\partial}{\partial t}\nabla^2\psi_2 + \frac{\partial}{\partial x}\psi_2 = -\epsilon\nabla^2\psi_2 + \delta_1 w_{12} \tag{15}$$

where δ_1 is the fractional upper layer depth and ϵ is the coefficient of bottom friction, then w_{12}, the vertical velocity at the interface acts as a 'wave-maker' associated with the baroclinic instability of the model Gulf Stream and recirculation. The forcing field w_{12} is a strongly varying function of space and time consequent on the rapidly evolving, highly non-linear eddies in the upper layer. It can be expressed in terms of an 'omega' equation thus

$$\gamma^2\nabla^2 w_{12} - H^* w_{12} = RJ\big(\psi_1 - \psi_2, \nabla^2(\psi_1 + \psi_2)\big) - (G_1 - G_2)$$

$$+ \frac{\partial}{\partial x}(\psi_1 - \psi_2) \tag{16}$$

where R is a Rossby number of the vorticity equation, $R = U_s/\beta L^2$, (U_s is a characteristic horizontal velocity, and L is the basin width, see Appendix), $H^* = H^2/H_1 H_2$ and $\gamma = L_\rho/L$ where $L_\rho = (g'H_1 H_2/f_0^2 H)^{1/2}$ is the Rossby radius and g' is the reduced gravity. However, because the deep flow is weak, the right-hand side of eqn. (16) does not depend strongly on ψ_2. Given a good analysis of the upper level synoptic-scale pressure field (proportional to ψ_1) the spatial and temporal variation of the vertical velocity can be deduced from eqn. (16) with imperfect knowledge of the ψ_2 field.

Equation (15) suggests that, given w_{12} from the 'omega' equation, the error in the lower layer streamfunction will propagate as a damped Rossby wave

$$\frac{\partial}{\partial t} \nabla^2 \Delta\psi_2 + \frac{\partial}{\partial x} \Delta\psi_2 = -\epsilon \nabla^2 \Delta\psi_2 \tag{17}$$

where $\Delta\psi_2 = \psi_2^T - \psi_2^A$, the truth minus the analysis streamfunctions. Equation (17) has solutions

$$\Delta\psi_2(t) = \Delta\psi_2(t_0) \, e^{-\epsilon(t-t_0)} \tag{18}$$

Thus any error in the initial conditions will decay with an e-folding time of $1/\epsilon = 55$ days, for the bottom friction coefficient used in our two-layer integration. The dashed line in Fig. 4 is the curve $\Delta\psi_2(t) = \Delta\psi_2(t_0)e^{-\epsilon(t-t_0)}$ where $t_0 = $ day 14 of the assimilation. By this time, after one repeat cycle, the error in the upper level streamfunction has dropped significantly, and so the w_{12} forcing the lower layer is quite close to the truth. The falling exponential curve models the decrease in the r.m.s.e. rather well, showing that the error in the lower layer streamfunction is well represented by a superposition of damped linear Rossby waves.

In order to further test our hypothesis, the effects of incomplete observations were eliminated by initializing the lower layer with no flow, as in Fig. 4, but replacing the upper layer streamfunction with the truth at all times over the whole basin ('infinite altimetry'). As shown in Fig. 6. the decrease in the lower layer r.m.s.e. is then given almost exactly by eqn. (18), this time with $t_0 = 0$.

4.4. Degraded models

Here a degraded model is used to assimilate our altimeter data. Two degradations will be considered, representing uncertainties in γ and R. We
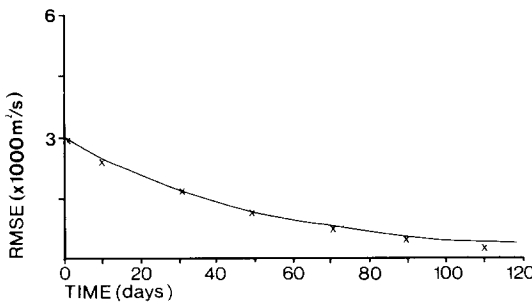
Fig. 6. Lower layer r.m.s.e. in a two-layer integration, initialized as in Fig. 2, in which the upper layer is replaced by the truth at all times over the whole grid ('infinite altimetry'). The crosses are values of the function $\Delta\psi_2(t = 0) \exp(-\epsilon t)$.
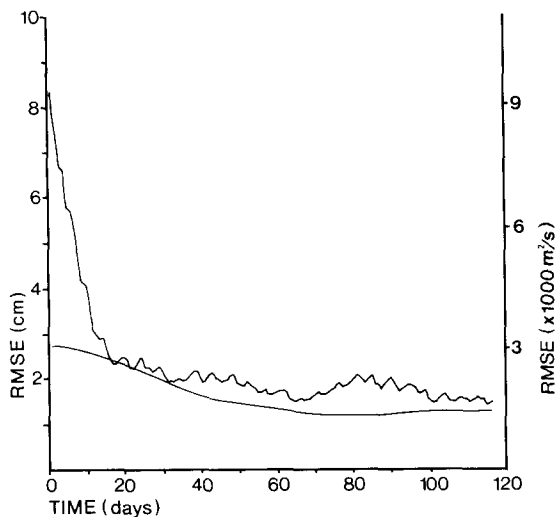
Fig. 7. Error curves for the ocean topography (in cm) and ψ_2 (in m^2 s^{-1}) obtained when perfect data from an optimum orbit repeat cycle (14 days) is assimilated into a two-layer model in which the stratification is in error; $g' = 2g'_{\mathrm{truth}}$ (initialization as in Fig. 2).

will see that their impact on the assimilation process as a constraint on the surface flow, and the ability of the model to interpolate vertically, can be understood in terms of the mechanism of transfer of information into the lower layer presented in the previous section. The degraded two-layer models were initialized with a Stommel solution in the upper layer, and zero motion beneath, and altimeter data from a satellite in an optimum orbit (repeat time 14 days, track spacing 140 km) assimilated as described previously. The resulting r.m.s.e. curves can therefore be compared directly with those in Fig. 2 (curve C) and Fig. 4, where a perfect model was used.

In the first degraded model, the density jump between the two layers has been doubled, giving $g' = 4 \times 10^{-2}$, increasing the Rossby radius L_ρ and hence γ by a factor of $2^{\frac{1}{2}}$; one might expect the assimilating model to produce anomalously large eddies. If altimetry is to constrain the upper layer circulation, then data must be supplied at a sufficiently high rate to compensate for this tendency.

The r.m.s.e. curves between the truth and degraded assimilation models shown in Fig. 7. for both upper and lower layer flows. They do not depart far from the r.m.s.e. curves shown in Fig. 2, indicating that our ability to deduce the surface flow from altimetry has not been significantly impaired when assimilating into a model whose stratification is in error. Thus it appears that if data are supplied on a 14-day repeat strategy, the rate of supply of information is sufficiently high to offset this particular model degradation.

A change in the stratification of the magnitude considered here has only a marginal impact on the ability of the model to interpolate vertically; the lower layer curve in Fig. 7. shows a slight increase in the r.m.s.e. over that obtained with a perfect model (cf. Fig. 4, curve B). This is consistent with our 'omega' eqn. (16). If $w_{12}(k)$ and $F(k)$ are the amplitudes of w_{12} and the right-hand side of eqn. (16) at wavenumber k, respectively, eqn. (16) can be written

$$k^2\gamma^2 w_{12}(k) + H^* w_{12}(k) = F(k)$$

The magnitude of w_{12} at wavenumber k is thus

$$w_{12}(k) = \frac{F(k)}{k^2\gamma^2 + H^*}$$

At long wavelengths, an increase in k will not change w_{12} significantly, whereas at shorter scales it will be reduced more noticeably: for $k \sim 1/100$ km, doubling g' results in $w_{12}(k)$ falling by 16%. The w_{12} forcing of the lower layer is less if γ is increased, and the effect is greatest on smaller scales (where altimetry is most effective). Thus in this example, where the stratification of the assimilating model is overestimated, the transfer of information into the subsurface layer is expected to be slower than for a perfect model, and the magnitude of the small-scale features underestimated.
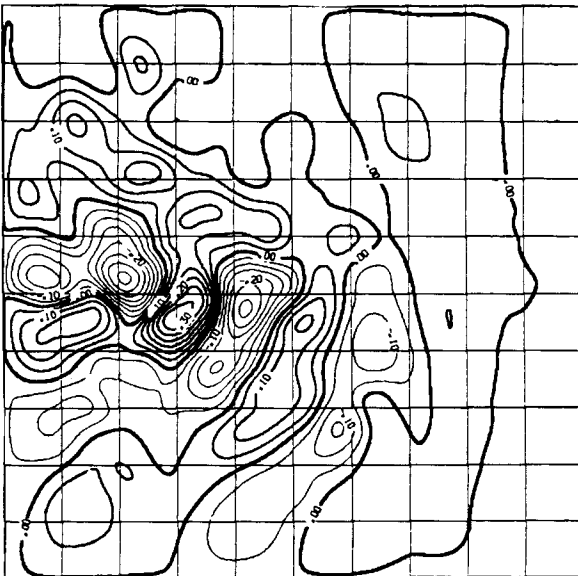
Fig. 8. The lower layer streamfunction (CI = 1500 m^2 s^{-1}) on day 108 of the two-layer integration in Fig. 7.
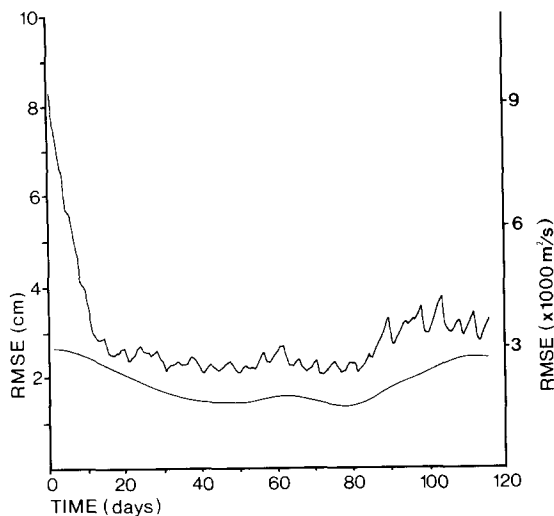
Fig. 9. Ocean topography (in cm) and ψ_2 (in m^2 s^{-1}) obtained when perfect data on an optimum orbit repeat cycle are assimilated into a two-layer model in which the non-dimensional parameter R has been increased to $(2^{\frac{1}{2}} R_{\text{truth}})$ (initialized as in Fig. 2).

Figure 7 indeed shows that after about 70 days the degraded model becomes less efficient than the perfect model at transferring information vertically; by this time the major features in the lower layer have been spun up, but errors in their magnitude are now noticeable. The lower layer streamfunction after 108 days of assimilation, shown in Fig. 8, is similar to the truth (Fig. 5a) except that the eddies are less intense; on scales of 100 km or so, magnitudes are reduced by about 20%. This is consistent with our mechanism for vertical interpolation discussed earlier.

In our second example, the assimilating model is degraded by increasing R by a factor of $2^{\frac{1}{2}}$. Thus the magnitude of the advection terms and the width of the inertial boundary current (which scales as $R^{1/2}$) is increased. One might expect that an advective velocity that is in error is likely to compromise severely the ability of the model to extrapolate information forward in time.

Figure 9 shows the r.m.s.e. between the truth and degraded model assimilation streamfunctions. The upper layer r.m.s.e. is consistently higher than when a perfect model is used (compare with Fig. 2a, curve C), and indeed after 80 days, altimetry is no longer able to constrain even the surface flow. The amplitude of the short period oscillations in the r.m.s.e. curve are a measure of how far the model deviates from truth in active areas between passes, and this increases as time goes on, indicating that the model is incapable of projecting data between repeat times, and is no longer providing useful first guess information.
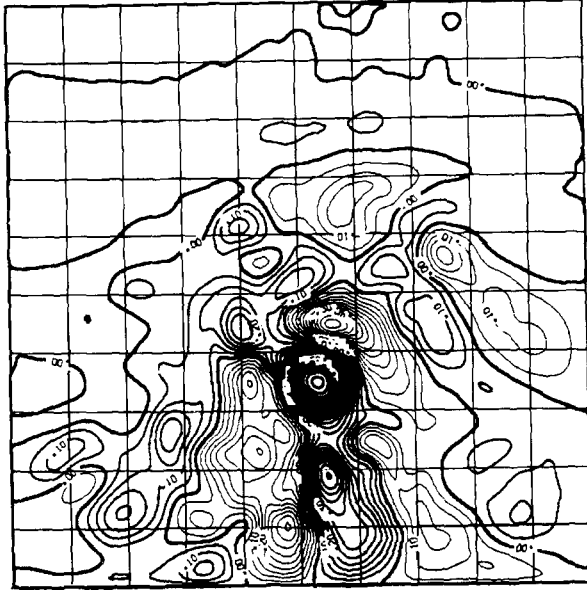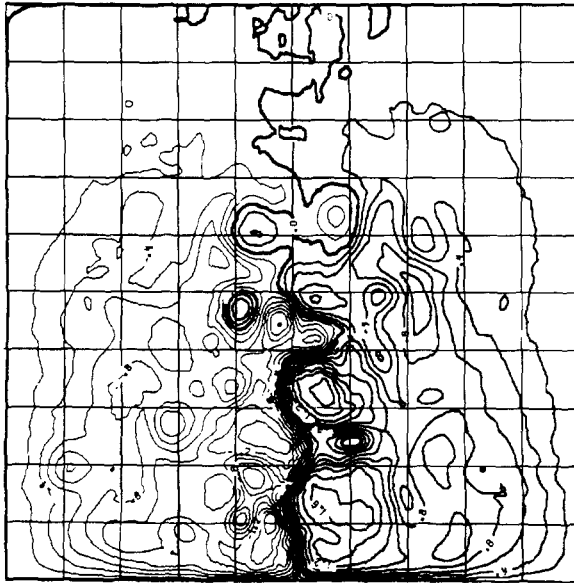
Fig. 10. Upper and lower layer streamfunctions on day 108 from the two-layer model in Fig. 9; CI = 5 cm (ocean topography) and 1500 m² s⁻¹ respectively.

ψ_1

ψ_2

The lower layer r.m.s.e. shown in Fig. 9 indicates that following an initial rapid transfer of information downward from the surface, accuracy is also lost in the deep flow. Figure 10 shows ψ_2 at 108 days and confirms that the subsurface flow cannot be successfully inferred by assimilating data at the surface of this degraded model. Once again, eqn. (16) provides the clue. The dominant term on the right-hand side (on eddy scales) is RJ (ψ_1, $\nabla^2\psi_1$), and so the lower layer will be forced by a w_{12} that is in error even if ψ_1 is perfectly specified.

These results emphasize the importance of the accurate representation of non-linear processes when assimilating into wind-driven models, especially if they are to be used to infer the deep flow. The effects of both model degradations discussed here are consistent with the mechanism for vertical interpolation formulated in the previous section, suggesting that the impact of other model degradations could be assessed by recourse to this theory.

4.5. Assimilation into multi-layer models

Having enquired into the behaviour of a two-layer model assimilating altimeter data at the surface, we now go on to consider whether a model of higher vertical resolution may be similarly constrained. The three-layer simulation of idealized ocean gyres studied by Marshall et al. (1988) is taken as our reference ocean. The model parameters, presented in the Appendix, were chosen to ensure that the internal jet has a realistic penetration scale. The upper layer (from which the altimeter data are taken, and into which they are assimilated) is 500 m deep, the middle 1000 m, whilst the deep flow is represented by a third layer 3500 m deep. The circulation is driven by a wind-stress curl of the same magnitude and form as in the two-layer integration. However, the higher vertical resolution of the model and the thinner upper layer results in a circulation which is unstable not only in the region of the jet but also in the interior. Figure 11 shows instantaneous streamfunction plots in each of the three layers (from the truth circulation at day 108).

In section 4.4, we described how, in a two-layer model, the deep flow comprises a superposition of essentially linear Rossby waves excited by the interfacial vertical velocity, which is controlled almost entirely by the upper layer flow. Errors in the initial conditions in the deep flow propagate as Rossby waves, damped by the Ekman friction on an e-folding time-scale of $1/\epsilon$. In the three-layer case, the deep third layer will respond to forcing by the interfacial velocity between it and the second layer in much the same way. We must first, however, consider the reduction of errors in the initial conditions of the second layer. The surface flow will drive the middle layer through vortex stretching but now the interfacial velocity w_{12} will depend on
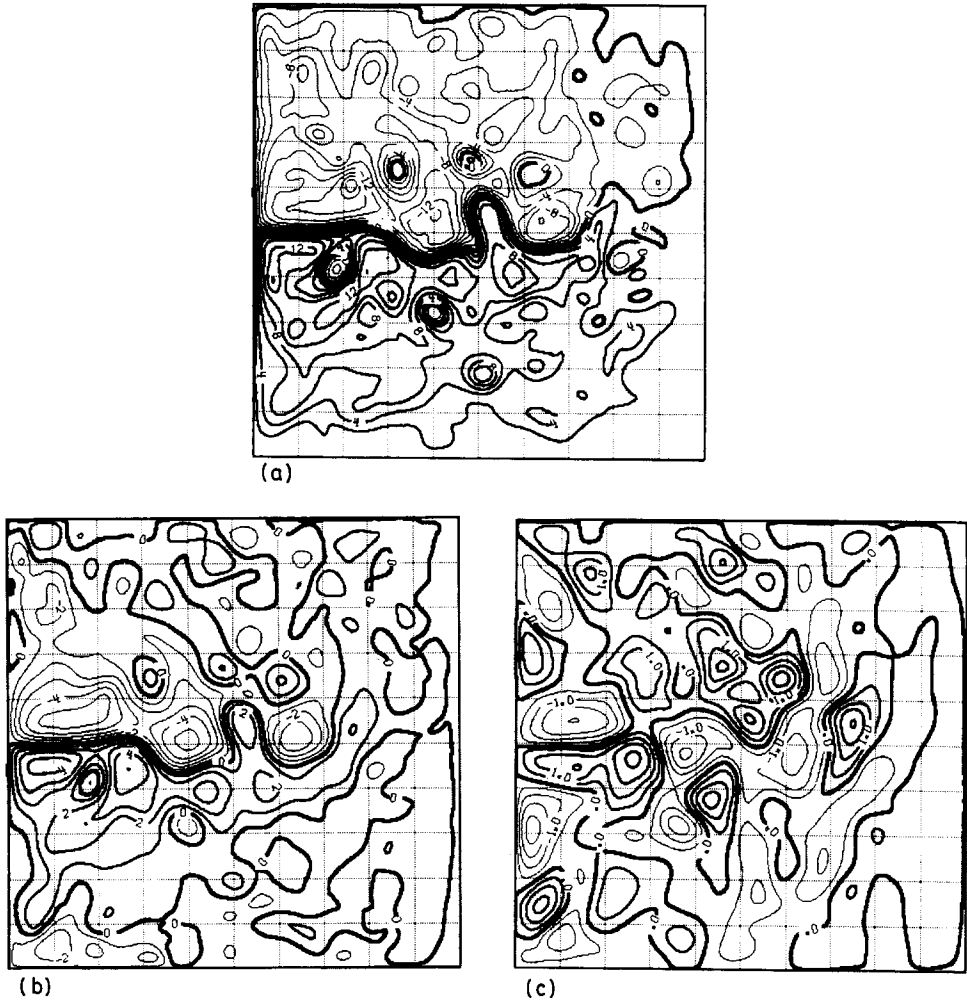
Fig. 11. (a) Upper (b) middle and (c) bottom layer streamfunctions from the truth three-layer model on day 108; CI = 4 cm (of ocean topography), 4200 m^2 s^{-1} and 2100 m^2 s^{-1} respectively.

the flow in both layers, and will not be controlled (as in the two-layer case) by ψ_1. In fact errors in the second layer may well adversely affect flow in the surface layer. Furthermore, since the only dissipative process in the second layer is a highly scale-selective bi-harmonic friction, only errors on the small (grid) scale will be damped rapidly.

Assimilation of data into the three-layer model on a 14-day repeat (optimum) orbit is not sufficient to constrain the model: truth and analysis diverge. Thus, in order to study the mechanism of vertical interpolation in
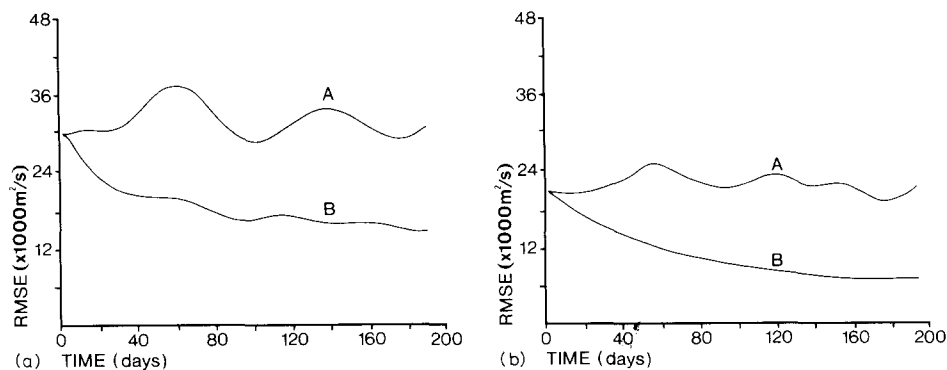
Fig. 12. Error curves (in $m^2\ s^{-1}$) obtained from a three-layer model that has been initialized with the 8-month truth climatology. Curve A is the variance of the truth about climatology, and curve B shows the r.m.s.e. between the model and truth streamfunctions where 'infinite altimetry' has been applied. (a) Second (middle) layer; (b) third (bottom) layer.

this three-layer case, results are presented from an assimilation experiment in which the surface layer is fully constrained by infinite altimetry; the upper layer streamfunction is replaced at all grid points and time steps by its truth value. The model was initialized from the (truth) 8-month time mean climatology. The r.m.s.e. curves (in $m^2\ s^{-1}$) between the streamfunction fields in layers two and three and the truth are shown in Fig. 12, together with the analysis streamfunction fields after 180 days of assimilation in Fig. 13. Note the difference in the vertical scale of Fig. 12(b) and that of Fig. 4 for the two-layer model; the basin-averaged variability in the three-layer model is much greater than in the two-layer case because now the abyssal eddy field almost fills the basin (cf. Fig. 11(c) with Fig. 5(a)). From Fig. 12, it can be seen that there has been some reduction in the error in both ψ_2 and ψ_3, although the fall is not nearly so rapid as in the two-layer case. After 180 days, the r.m.s.e. in the second layer has fallen to 50% of its initial value (the e-folding time is approximately 150 days). The deep flow r.m.s.e. falls to 40% of its original value, with an e-folding time of 110 days. In this integration, $1/\epsilon = 74$ days, so our model of error reduction as a damped linear Rossby wave does not seem to be appropriate here. Evidently non-linearities in the second layer severely inhibit the vertical transfer of information from the surface to the deep layer. However, it should be stressed that there is still some error reduction: many of the features in both subsurface layers have been inferred correctly, as can be seen by comparing Fig. 13 with Fig. 11.

It can be concluded, then, that if surface pressure data are assimilated into models with more than two layers the ability of the model to spin up

ψ_1 $\qquad\qquad\qquad\qquad\qquad\qquad\qquad\qquad$ ψ_2
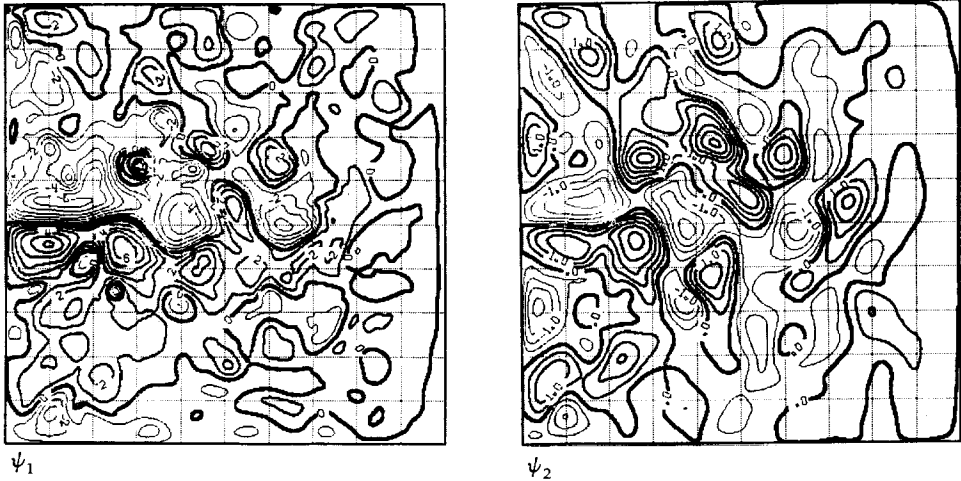
Fig. 13. Second and third layer streamfunction plots on day 108 with 'infinite altimetry' for the three-layer model of Fig. 11; CI = 4200 m^2 s^{-1} and 2100 m^2 s^{-1} respectively.

the deep layers is severely diminished. In the absence of further information a single altimeter cannot constrain a multi-layer model, even when flown in an optimum repeat orbit. It should be emphasized, however, that here no attempt has been made to use statistical techniques (for example vertical structure functions) to extrapolate surface information into deeper layers or dynamical methods (for example, projecting onto vertical modes as proposed by Webb and Moore (1986)). Neither has the use of subsurface *in situ* observations been considered in conjunction with altimetry. Each of these possibilities deserves further work.

5. DISCUSSION

Our investigation is presented very much in the spirit of the early network studies directed at optimizing and evaluating the meteorological observing network. Rather than focusing on a limited geographical area (as for example in the work reviewed by Robinson (1986), or the study of De Mey and Robinson (1987)) we have considered assimilation into basin-scale models. It is only the advent of radar altimetry that makes this a tenable possibility. It is recognized that in order to obtain an altimetric measurement of the ocean topography that is sufficient to determine the mean circulation, a geoid vastly more accurate than is currently available is needed. However, the geoid is being continually refined (indeed, in regions where our knowledge of the ocean circulation is good, the latter can be used

in conjunction with altimetry to improve the geoid (see Thompson, 1986)). Here is has been assumed that the geoid is sufficiently well known to allow determination of the surface pressure field from altimetry. We have investigated the assimilation into a model of surface pressure field data on space and time-scales obtainable from a single radar altimeter, and assessed the degree to which such information may constrain that model.

The following general conclusions can be drawn.

(1) Observations of the surface pressure field on space and time-scales possible with a single satellite-borne radar altimeter provide strong constraints on baroclinic, eddy resolving ocean circulation models, both at the surface and in deeper layers.

(2) The skill of the surface is a strong function of the spatial and temporal frequency of the altimetric observations, and is only weakly dependent on the random error in the instrument (for reasonable levels of noise). For synoptic mapping on basin scales, an orbit repeat time of about 14 days is found to be optimum.

(3) The dynamical mechanism by which information at the surface is extrapolated vertically, constraining abyssal flows, can be understood readily in two-layer models in which the deep flow is a superposition of damped linear Rossby waves forced by vortex stretching at the interface between the layers. Given a good analysis of the surface pressure field, the forcing of the lower layer can be determined, and so any initial error decays as a damped Rossby wave with an Ekman spin-down time-scale. However, in more realistic models, where many shallow layers are required to represent the strongly depth-dependent currents in the upper levels of the wind-driven gyre, they are less able to spin-up subsurface flows from information provided at the surface.

Finally, it must be stressed that altimetry should be seen as only one, albeit central, component of planned observing networks. Future studies should assess the impact of altimetry in conjunction with both complementary *in situ* observations (for example, velocity observations at thermocline depth from neutrally buoyant floats) and other remotely sensed information, particularly sea-surface temperature and ocean colour sensors giving the positions of major fronts and eddies.

APPENDIX

The potential vorticity equation (non-dimensionalized)

$$\frac{1}{R}\frac{\partial q_n}{\partial t} + J(\psi_n, q_n) = G_n \tag{A1}$$

is integrated forward numerically (Brugge et al., 1987) for each layer ($n = 1$, 2 or 3) on a finite-difference grid in a square domain, where q_n is the quasi-geostrophic potential vorticity, ψ_n is the streamfunction, G_n is the potential vorticity forcing function, $J(a, b)$ is the Jacobian of a and b, $\partial a/\partial x\, \partial b/\partial y - \partial b/\partial x\, \partial a/\partial y$, and x ($0 \le x \le 1$) is east, $y(-0.5 \le y \le 0.5)$ is north and t is time.

The potential vorticity is related to the streamfunction through

$$\mathbf{q} = R\nabla^2\mathbf{\Psi} + \mathbf{y} - \mathbf{S}\mathbf{\Psi} \tag{A2}$$

where

$$\mathbf{q} = \begin{pmatrix} q_1 \\ q_2 \\ q_1 \end{pmatrix}; \qquad \mathbf{\psi} = \begin{pmatrix} \psi_1 \\ \psi_2 \\ \psi_1 \end{pmatrix}$$

and $\mathbf{S}$ is the stretching matrix given by

$$\mathbf{S} = \frac{RL^2}{L_T^2}\begin{pmatrix} \dfrac{1}{\delta_1\Delta\sigma_{21}} & \dfrac{-1}{\delta_1\Delta\sigma_{21}} & 0 \\ \dfrac{-1}{\delta_2\Delta\sigma_{21}} & \dfrac{1}{\delta_2\Delta\sigma_{21}} + \dfrac{1}{\delta_2\Delta\sigma_{32}} & \dfrac{-1}{\delta_2\Delta\sigma_{32}} \\ 0 & \dfrac{-1}{\delta_3\Delta\sigma_{32}} & \dfrac{1}{\delta_3\Delta\sigma_{32}} \end{pmatrix} \tag{A3}$$

In Eqns. (A1)–(A3), length has been non-dimensionalized with respect to L, where L is the north–south extent of the basin; depth with respect to H the depth of the ocean; time with respect to $(\beta L)^{-1}$, where β is the planetary vorticity gradient; ψ with respect to $U_S L$, where U_S is a characteristic velocity chosen to be the Sverdrup velocity $U_S = f_0 W_{EK}/\beta H$ and W_{EK} is an Ekman pumping velocity; q with respect to βL. f_0 is the reference Coriolis parameter.

The coefficient $R = U_S/\beta L^2$ is a Rossby number for the vorticity equation; $L_T = (gH/1000 f_0^2)^{1/2}$ is a pseudo-Rossby radius, $\Delta\sigma_{n+1,n} = 10^3\Delta\rho_{n+1,n}/\rho_0$ expresses the density jumps between the layers in σ units where

$$\Delta\rho_{n+1,n} = \rho_{n+1} - \rho_n$$

and $\delta_n = H_n/H$ are the fractional layer depths.

The Gs in eqn. (A1) are given by

$$G_1 = \frac{1}{\delta_1} W_0 - \nu \nabla^6 \psi_1$$

$$G_2 = -\nu \nabla^6 \psi_2$$

$$G_3 = -\nu \nabla^6 \psi_3 - \epsilon \nabla^2 \psi_3$$

where W_0 is the (non-dimensionalized) vertical velocity at the base of the Ekman layer in units of W_{EK} and W_0 is chosen to be

$$W_0 = \sin 2\pi y$$

driving the model in a double-gyre configuration. The coefficients ν and ϵ are lateral and bottom diffusion constants respectively.

Parameters

General: $L = 3 \times 10^6$ m, $\beta = 10^{-11}$ m^{-1} s^{-1}

Two-layer: $H_1 = 1000$ m
$H_2 = 4000$ m
$\Delta\sigma_{12} = 2$
$f_0 = 7.0 \times 10^{-5}$ s^{-1}
$\epsilon = 55$ days^{-1}
$U_S = 1.4 \times 10^{-3}$ ms^{-1}
$R = 1.6 \times 10^{-5}$
Rossby radius = 48 km

Three-layer: $H_1 = 500$ m
$H_2 = 1000$ m
$H_3 = 3500$ m
$\Delta\sigma_{12} = 2$
$\Delta\sigma_{23} = 1$
$f_0 = 7.0 \times 10^{-5}$ s^{-1}
$\epsilon = 74$ days^{-1}
$U_S = 1.4 \times 10^{-3}$ ms^{-1}
$R = 1.6 \times 10^{-5}$
Rossby radius = 48 and 18 km

REFERENCES

Brugge, R., Nurser, A.J.G. and Marshall, J.C., 1987. A Quasi-geostrophic Ocean Circulation Model. Internal report, Imperial College London.

Cheney, R.E. and Marsh, J.G., 1981. Oceanographic evaluation of geoid surfaces in the Western North Atlantic. In: J.F.R. Gower (Editor), Oceanography from Space, Plenum, New York, pp. 855–864.

De Mey, P. and Robinson, A.R., 1987. Assimilation of altimeter eddy fields into a limited-area quasi-geostrophic model. J. Phys. Oceanogr., 17: 2280–2293.

Eliassen, A., 1954. Provisional report on calculation of spatial covariance and autocorrelation of the pressure field. Inst. Weather and Climate Research, Academy of Sciences, Oslo, Rep. No. 5.

Gandin, L.S., 1965. Objective Analysis of Meterological Fields (1963). Translated from Russian by the Israeli Program for Scientific Translations.

Ghil, M, Cohen, S. Tavantzis, J., Bube, K. and Isaacson, E., 1981. Applications of estimation theory to numerical weather prediction. In: L. Bengtsson, M. Ghil and E. Källén (Editors),

Dynamical Meteorology: Data Assimilation Methods. Springer-Verlag, New York, pp. 139–224.

Haidvogel, D.B. and Rhines, P.B., 1983. Waves and circulation driven by oscillatory winds in an idealised ocean basin. Geophys. Astrophys. Fluid Dyn., 25: 1–63.

Hollingsworth, A., 1984. Meteorological data analysis. European Centre for Medium Range Weather Forecasts. Lecture Note No. 2.2, Chapter 6.

Hurlbert, H.E, 1985. Dynamic transfer of simulated altimeter data into subsurface information by a numerical model. J. Geophys. Res., 91 (C2): 2372–2400.

Jackson, D.D., 1979. The use of a priori data to resolve non-uniqueness in linear inversion. Geophys. J. R. Astron. Soc., 57: 137–157.

Marshall, J.C., 1985a. Determining the ocean circulation and improving the geoid from satellite altimetry. J. Phys. Oceanog., 15: 330–349.

Marshall, J.C., 1985b. Altimetric observing system circulation studies with an eddy-resolving ocean circulation model. Proceeding of a Workshop on Satellite Data and its use in Climate Models, Alpbach, 10–12 June, European Space Agency ESAP-244, pp. 73–76.

Marshall, J.C., Nurser, A.J.G. and Brugge, R., 1988. On the time-average flow of quasi-geostrophic wind-driven gyres. J. Geophys. Res., 93: 15427–15436.

Rhines, P.B. and Holland, W.R., 1979. A theoretical discussion of eddy-driven mean flows. Dyn. Atmos. Oceans, 3: 289–325.

Rienecker, M.M., Mooers, C.N.K. and Robinson, A.R., 1987. Dynamical interpolation and forecast of the evolution of mesoscale features off north California. J. Phys. Oceanog., 17: 1189–1213.

Robinson, A.R., 1986. Data assimilation, meso-scale dynamics and dynamical forecasting. In: J.J.O. Brien (Editor), Advanced Physical Oceanographic Numerical Modelling, Reidel Press, Dordrecht.

Rodgers, C.D., 1976. Retrieval of atmospheric temperature and composition from remote measurements of thermal radiation. Rev. Geophys. Space Phys., 14: 609–624.

Stommel, H., 1948. The westward intensification of wind-driven ocean currents. Trans. Am. Geophys. Union, 29: 202–206.

Thompson, J.D., 1986. Altimeter data and geoid error in mesoscale ocean prediction; some results from a primitive equation model. J. Geophys. Res., 91: 2401–2417.

Webb, D.J. and Moore, A., 1986. Assimilation of altimeter data into ocean models. J. Phys. Oceanogr., 16: 1901–1913.

Wunsch, C., 1978. The North Atlantic general circulation west of 50°W determined by inverse methods. Rev. Geophys. Space Phys., 16: 583–620.